Vibrational properties of tin clathrate materials

Charles W. Myles,[1] Jianjun Dong,[2] Otto F. Sankey,[3] C. A. Kendziora,[4] and G. S. Nolas[5]
[1]*Department of Physics, Texas Tech University, Lubbock, Texas 79409-1051*
[2]*Department of Physics, Auburn University, Auburn, Alabama 36849-5311*
[3]*Department of Physics and Astronomy and Materials Research Center, Arizona State University, Tempe, Arizona 85287*
[4]*Materials Science and Technology Division, Code 6330, Naval Research Laboratory, Washington, D.C. 20375*
[5]*Department of Physics, University of South Florida, Tampa, Florida 33620*
(Received 16 October 2001; revised manuscript received 5 April 2002; published 11 June 2002)

We have performed density functional calculations of the vibrational modes of three tin-based, cagelike clathrate materials: the pure type-I (Sn_{46}) and type-II (Sn_{136}) frameworks, and the donor/acceptor compensated compound $Cs_8Ga_8Sn_{38}$. We have also theoretically identified the infrared- and Raman-active modes in these materials and have computed their Raman spectra. In addition, we report measurements of the Raman spectrum of $Cs_8Ga_8Sn_{38}$ and compare the experimental spectrum with the theoretical one. By this means, we are able to unambiguously identify the low-frequency ''rattling'' vibrational modes in this material, which are due to the motion of the Cs atoms that are loosely bound in the Sn cages.

DOI: 10.1103/PhysRevB.65.235208 PACS number(s): 78.30.−j, 63.20.−e

I. INTRODUCTION

The ground state crystalline structure of C, Si, Ge, and Sn is the tetrahedrally bonded, sp^3 diamond structure. With the exception of C, these elements can also form metastable, expanded volume structures called clathrates. These are open-framework structures in which the lattice contains 20-, 24-, and 28-atom cages, and in which all atoms are in a *fourfold-coordinated* sp^3 configuration. The local bonding is thus similar to that in the diamond structure; however the clathrates have pentagonal rings, which makes the topology quite different from that of the diamond structure. Further, the cages can house ''guest'' atoms, and the choice of guest may be used to tune the properties of the material, including the vibrational properties.

In this paper, we extend our previous[1] density functional–based theoretical study of the structural and electronic properties of some of the tin-based clathrates to include their vibrational properties. We have calculated the lattice vibrational spectra of the pure type-I (Sn_{46}) and type-II (Sn_{136}) clathrate frameworks, and of the compound $Cs_8Ga_8Sn_{38}$. For this material, the Cs atoms are guests inside the clathrate cages. This compound is interesting because of the possible existence of ''rattler'' vibrational modes due to the Cs motion. We have also theoretically identified the infrared- and Raman-active modes in these materials and have computed their Raman spectra. In addition, we also report measurements of the Raman spectra of $Cs_8Ga_8Sn_{38}$ and show that the measured and calculated spectra for this material compare quite favorably. By using a combined theoretical-experimental analysis of the Raman spectra, we are able to unambiguously identify the low-frequency, vibrational rattling modes associated with the Cs guests.

Clathrate phases of Si and Ge, with guest atoms encapsulated in the cages, have been known for at least 37 years.[2–7] On the other hand, Sn clathrates have only recently been synthesized.[8–11] There has recently been considerable experimental and theoretical research on semiconductor clathrates. This is due mainly to the expected new and tunable properties of these materials. This tunability is mainly due to the presence of the cages and of the guests that may be within them. In addition, other atoms can be ''alloyed'' on the framework sites, and this can cause a rich variety of changes in the properties. Silicon clathrates have been the most studied of this class. Theoretical studies of both Si (Refs. 12–17) and Ge (Refs. 18 and 19) clathrates have been made by several groups.

A technological motivation for the study of the clathrates is their potential use as thermoelectrics. A good thermoelectric must simultaneously have a high Seebeck coefficient, a high electrical conductivity, and a low thermal conductivity.[20] These properties are not independent, so it is difficult to satisfy all of these conditions simultaneously. A thermoelectric design concept, which can potentially reduce the thermal conductivity, is to introduce impurities or guests into the framework cages, which can produce ''rattling'' vibrational modes.[21–23] Testing this idea on the clathrates, Nolas *et al.*[24,25] have shown that a Ge-based clathrate ($Sr_8Ga_{16}Ge_{30}$) has a very low thermal conductivity. Recent simulations[26,27] have also shown that type-I Ge clathrate frameworks containing guest ''rattlers'' have comparable thermal conductivities to that of amorphous Ge, as was suggested by Slack[20,21] and as has been observed experimentally.[25,28] Recently, low thermal conductivities in some Sn-based clathrates have been also reported by Nolas *et al.*[9–11]

II. COMPUTATIONAL DETAILS

The two pure clathrate frameworks are the simple cubic type-I and the face-centered cubic type-II structures. These, respectively, contain 46 and 136 atoms per cubic unit cell. For the Sn clathrates, these are Sn_{46} and Sn_{136}. The structure of $Cs_8Ga_8Sn_{38}$ is based upon that of Sn_{46}, with each of the 20- and 24-atom cages occupied by guest Cs's and eight of the Sn sites occupied by Ga's to compensate for the Cs charge. To avoid the problem of treating a random Sn/Ga alloy, following Ref. 1, we have constructed a symmetric,

ordered model for this compound. The geometry of this model reduces the point group symmetry from O_h to T_d.

Further details of the crystalline structures for Sn_{46}, Sn_{136}, and $Cs_8Ga_8Sn_{38}$ are given in Ref. 1. These optimized equilibrium structures are the starting points for our calculations of the vibrational modes of these materials. Both the calculations of Ref. 1 and the present calculations are based on the local density approximation (LDA) and use a plane-wave basis with ultrasoft pseudopotentials.[29,30] The Vienna *ab initio* simulation package[31,32](VASP) has been used with the Ceperley-Alder functional[33] to approximate the exchange-correlation energy. The LDA-optimized energy minima, equilibrium volumes, lattice constants, and internal coordinates for the materials considered here may be found in Tables II–IV of Ref. 1. In Ref. 1, it is also shown that all three materials are semiconductors.

Starting with the LDA-optimized structures, obtaining the lattice vibrational dispersion relations requires a calculation of the dynamical matrix, $D(\vec{q})$ ($\vec{q}$ is a wave vector in the first Brillouin zone). Diagonalization of $D(\vec{q})$ gives the eigenvalues and eigenvectors. Starting with a force-free, optimized unit cell, the calculations are performed in two steps: the first step obtains the $\vec{q}=\vec{0}$ modes exactly (within the harmonic approximation) and the second step approximately obtains the $\vec{q}\neq\vec{0}$ modes. These procedures have been discussed in detail in previous papers,[16,18] so they are only briefly outlined here.

First, $\phi(\vec{q}=\vec{0})$, the $3N\times 3N$ $\vec{q}=\vec{0}$ force constant matrix (N is the number atoms in supercell) is calculated. A row of matrix elements of $\phi(\vec{q}=\vec{0})$ is found by computing the forces generated on each atom when an atom is displaced a distance U_0 from equilibrium, and by dividing these forces by U_0. In general, $3N$ displacements must be made, but symmetry dramatically reduces this number. The symmetry-unique displacements used for the structures considered here are described in Secs. IV A and V A. The $\vec{q}=\vec{0}$ dynamical matrix, $D(\vec{q}=\vec{0})$, is obtained from $\phi(\vec{q}=\vec{0})$ in the standard manner[39] and is then diagonalized to obtain the $\vec{q}=\vec{0}$ eigenvalues and eigenvectors. This procedure is exact within the harmonic approximation. Raman and ir experiments probe vibrational modes near $\vec{q}=\vec{0}$, so this procedure also generates the Raman- and ir-active modes.

Second, an approximate $\vec{q}\neq\vec{0}$ dynamical matrix, $D(\vec{q})$, is computed by assuming that the matrix elements of the real-space force constant matrix, $\phi(\vec{r})$, decay rapidly with increasing distance $\vec{r}$ between atoms and become negligible for two atoms separated by a distance greater than third- nearest neighbors ($\geqslant 6$ Å). Since Sn-based clathrate crystals have large unit cells, this fast-decay assumption allows us to approximate the force constants between two ''nearby'' atoms (i.e., at distances smaller than $\sim$ half the unit-cell size) with the matrix elements of the $\vec{q}=\vec{0}$ force constant matrix, and to set the force constants between two ''distant'' atoms (i.e. at distances larger than $\sim$ half the unit-cell size) to zero. This allows an approximate calculation of (a ''truncated'') $\phi(\vec{r})$ from $\phi(\vec{q}=\vec{0})$. From this $\phi(\vec{r})$, $\phi(\vec{q})$ is constructed by performing a lattice/basis sum. The $D(\vec{q})$ matrix is then constructed by doing a mass-modified Fourier transformation of the ''truncated'' force constant matrix $\phi(\vec{r})$. Finally, $D(\vec{q})$ is diagonalized to obtain the eigenvalues and eigenvectors for $\vec{q}\neq\vec{0}$.

Thus, only the $\vec{q}=\vec{0}$ vibrational modes are calculated exactly, and those at $\vec{q}\neq\vec{0}$ are approximate. For the diamond structure, we have found that this approximation is worst for the transverse acoustic modes. The error could be reduced by calculating $\phi(\vec{q}=\vec{0})$ for a larger supercell to enlarge the real-space truncation range. With current workstations, for the clathrates, this type of calculation is computationally impractical for an LDA plane-wave calculation, and offers little benefit.

This method assumes that the harmonic approximation is valid. This must be carefully checked in methods that use finite displacements, U_0. Except for the modes associated with Cs guests in the large cages in $Cs_8Ga_8Sn_{38}$ (Sec. V A), we have used $U_0=0.02$ Å. Also, we calculate $\phi(\vec{q})$ with both $+U_0$ and $-U_0$ and average the two matrices. Any odd-order anharmonicity then vanishes, leaving only fourth- or higher- (even) order anharmonic errors.

The intensity of first-order Raman scattering is proportional to the square of the polarization change with atomic displacement. Here, as in Ref. 18, we estimate the Raman scattering intensity[34] using a bond-polarizability model (BPM).[35] The BPM describes the bond polarization in terms of polarization expansion coefficients along the bond direction and normal to the bond. This model has been successful for diamond-structure C, Si, and Ge.[35,36] Previously, we have found that the parameters for these systems are not transferable to new geometries.[16,18] In our application of this model to the Sn clathrates, we have modified the parameters empirically.[37] Thus, while our predictions of the Raman *frequencies* are accurate within the discussed approximations, our predicted *intensities* are only qualitative. We note that, for Ge clathrates, the experimental Raman-active modes[11] are in excellent agreement with the theoretical calculations of Dong *et al.*[38]

III. EXPERIMENTAL DETAILS

The $Cs_8Ga_8Sn_{38}$ specimen was synthesized as described previously.[10] High-purity elements were reacted inside a tungsten crucible in an argon atmosphere for two weeks at 550 °C. The resulting compound consisted of small crystallites, which were ground to fine powders and hot pressed inside graphite dies at 380 °C and 170 MPa for two hours in an argon atmosphere. The resulting dense pellet was analyzed using x-ray diffraction and an electron-beam microprobe to confirm the stoichiometry. The pellet was then cut with a wire saw and polished for Raman scattering measurements.

Raman scattering measurements on $Cs_8Ga_8Sn_{38}$ were made using the 514.5 nm line of an Ar^+ laser. Spectra were measured at 10 K ambient temperature. However, the inci-

dent power (typically 50 mW) was sufficient to heat the sample due to the low thermal conductivity. The samples were placed in a helium atmosphere to eliminate extraneous Raman signals from air. The collected scattered light was dispersed using a triple grating spectrometer (Dilor) with a resolution set to 3 cm^{-1} and was detected by a liquid nitrogen–cooled charge-coupled device array. The lower cutoff frequency of the band-pass filter was set at 20 cm^{-1}. Although the samples were polycrystalline, differences in the spectra were observed by selecting the scattered polarization parallel or orthogonal to the incident polarization.

IV. ELEMENTAL CLATHRATE FRAMEWORK MATERIALS

A. Vibrational dispersion relations

We have made considerable use of symmetry in implementing the procedure of Sec. II to obtain the vibrational spectra. For Sn_{46}, which has O_h point group symmetry, only six independent displacements U_0 need to be made. [Actually, 12 displacements are made, since $\phi(\vec{q})$ is computed for both $+U_0$ and $-U_0$ and the results are averaged.] These are a single displacement of an atom at a 16*i* site, two orthogonal displacements of an atom at a 6*c* site, and three orthogonal displacements of an atom at a 24*k* site. Group theory generates the remaining $(3\times46)-6=132$ columns of $\phi(\vec{q})$. For Sn_{136}, which also has O_h point group symmetry, only four displacements U_0 need to be made (eight for both positive and negative U_0) instead of 102 $(=3\times34)$ displacements.

The calculated dispersion curves for Sn_{46} and Sn_{136} are shown in Figs. 1(a) and 1(b). The small Brillouin zone coming from the large unit cells causes narrow vibrational bands. In both materials there exist two high density of states regions. One is just above the acoustic phonon branches ($\sim$40 cm^{-1} to 65 cm^{-1}) and the other is at the top of optical bands ($\sim$175 cm^{-1} to 190 cm^{-1}). The optical bands are very flat, as is reminiscent of ''zone folding.'' Thus, most optical modes, except for a few within the $\sim$60–160 cm^{-1} region, have very small group velocities $[d\omega(\vec{q})/d\vec{q}]$. According to heat transport theory,[39–41] phonons with small velocities transfer heat inefficiently. This suggests that pure Sn clathrates should have a lower thermal conductivity than diamond phase α-Sn. Our work on the thermal conductivity of Ge clathrates[26,27] has shown that this suggestion has validity.

The optical modes for Sn_{46} and Sn_{136} are located from $\sim$40 cm^{-1} to $\sim$194 cm^{-1}. For comparison, the highest experimental optical mode in α-Sn is at $\sim$201 cm^{-1}.[42] Starting with an LDA-optimized, equilibrium α-Sn lattice,[1] we have calculated this frequency and have found 187.8 cm^{-1}, an underestimate in comparison with experiment.

B. $\vec{q}=\vec{0}$ modes; ir and Raman-active modes; Raman spectra

Infrared (ir) and Raman scattering probe the Γ point ($\vec{q}=\vec{0}$) phonon modes. To guide possible experiments, we have

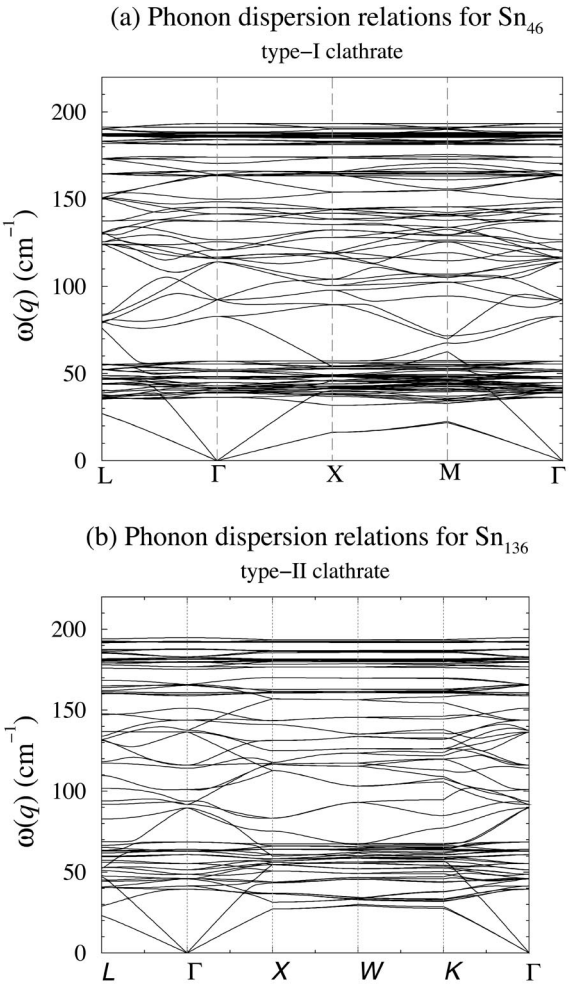

FIG. 1. Phonon dispersion relations for (a) Sn_{46} and (b) Sn_{136}.

examined the frequencies and symmetries of the $\vec{q}=\vec{0}$ modes in Sn_{46} and Sn_{136}. Our results for Sn_{46} are listed in the left four columns of Table I and those for Sn_{136} are listed in the right four columns of that table. Zero frequency translational modes are not included. Owing to symmetry-related degeneracy, the $138=(3\times46)$ Γ-point phonon modes in Sn_{46} have only 57 distinct frequencies. From group theory, the symmetries of these are $3A_{1g}+4A_{2g}+7E_g+8T_{1g}+8T_{2g}+2A_{1u}+2A_{2u}+4E_u+10T_{1u}+9T_{2u}$. Similarly, in Sn_{136}, there are 42 distinct frequencies, which have the symmetries

$$3A_{1g}+1A_{2g}+4E_g+5T_{1g}+8T_{2g}+1A_{1u}+3A_{2u}+4E_u+8T_{1u}+5T_{2u},$$

and which come from the $102=(3\times34)$ Γ-point modes.

Group theory[43] has been used to determine the allowed Raman and ir modes. These are denoted by a check mark in the appropriate column in Table I. Some ir- and Raman-active modes may have intensities which are too small to be detected, so the number of experimentally observed frequencies may be fewer than the predicted number of active modes.

TABLE I. Γ-point ($\vec{q}=\vec{0}$) phonon modes of Sn_{46} and Sn_{136}. The unique frequencies are listed, along with their symmetries. The Raman or ir activity of a mode is denoted by a check mark (√) in the appropriate column.

Sn_{46}				Sn_{136}			
Frequency (cm^{-1})	Symmetry	Raman active	ir active	Frequency (cm^{-1})	Symmetry	Raman active	ir active
35.7	T_{2g}	√		39.5	T_{2g}	√	
38.7	T_{1g}			40.6	T_{1g}		
41.2	A_{2u}			41.3	E_g	√	
41.4	T_{1g}			44.6	T_{1g}		
44.6	E_u			46.5	T_{2u}		
45.2	T_{2g}	√		48.8	E_u		
45.7	T_{1u}		√	49.1	T_{2u}		
46.7	T_{2u}			50.6	T_{1g}		
47.6	E_g	√		50.9	A_{2g}		
47.8	T_{1g}			52.3	T_{1u}		√
49.0	E_u			56.9	T_{2g}	√	
49.0	A_{2g}			60.4	T_{1u}		√
49.7	T_{2u}			98.8	T_{1u}		√
50.2	T_{1u}		√	100.3	T_{2g}	√	
51.9	T_{1g}			106.2	A_{2u}		
54.9	T_{2g}	√		108.4	E_u		
55.1	T_{1u}		√	122.4	A_{1g}	√	
81.5	E_g	√		123.4	T_{2g}	√	
89.8	T_{2u}			137.6	E_g	√	
91.6	A_{2g}			138.5	T_{2u}		
115.8	T_{1u}		√	144.5	T_{1u}		√
116.6	T_{2g}	√		153.2	A_{2u}		
117.3	E_g	√		155.6	A_{1g}	√	
122.7	T_{2u}			156.5	T_{2g}	√	
125.1	A_{1g}	√		162.5	A_{2u}		
125.5	A_{1u}			162.8	T_{1g}		
137.7	T_{1g}			164.9	T_{1u}		√
141.9	T_{2u}			175.8	E_u		
145.7	T_{1u}		√	178.7	A_{1g}	√	
147.9	A_{2u}			179.1	T_{2u}		
149.3	A_{2g}			180.2	T_{1u}		√
161.6	T_{2g}	√		181.0	E_u		
162.6	E_g	√		182.6	E_g	√	
164.0	T_{1u}		√	182.8	T_{2g}	√	
165.1	T_{1g}			185.6	T_{1g}		
168.6	A_{1g}	√		186.0	T_{2g}	√	
173.6	T_{2u}			188.6	E_g	√	
180.5	T_{1u}		√	190.1	A_{1u}		
183.3	E_g	√		190.6	T_{1u}		√
183.8	T_{2u}			191.9	T_{2u}		
185.1	E_u			193.1	T_{2g}	√	
185.4	T_{2g}	√					
185.9	T_{1u}		√				
186.0	A_{1u}						
186.2	T_{1g}						
186.8	E_u						
186.9	E_g	√					

TABLE I. *(Continued)*

Sn_{46} Frequency (cm^{-1})	Sn_{46} Symmetry	Sn_{46} Raman active	Sn_{46} ir active	Sn_{136} Frequency (cm^{-1})	Sn_{136} Symmetry	Sn_{136} Raman active	Sn_{136} ir active
187.0	T_{2g}	√					
187.7	T_{1g}						
188.3	T_{2u}						
188.5	A_{1g}	√					
188.8	T_{2g}	√					
191.1	T_{2u}						
191.8	T_{1u}		√				
193.4	E_g	√					
193.7	A_{2g}						

To obtain an idea about the expected shape of the Raman spectra, we have used the BPM, discussed in Sec. II B, to estimate the Raman *intensities* for these materials. The empirical parameters used have been chosen[37] using the rule found for Si (Ref. 16) and Ge (Ref. 18). We have assumed a parallel polarization I_{xx} (VV), which accesses all Raman-active modes. The results have been averaged over a 4π solid angle to represent powderlike samples. The resulting spectra for Sn_{46} and Sn_{136} are shown in Figs. 2(a) and 2(b), respectively. Each peak can be identified with one or more of the Raman-active modes in Table I. We again note that the frequencies are *exact* within the approximations of Sec. II, but that the intensities are *qualitative*.

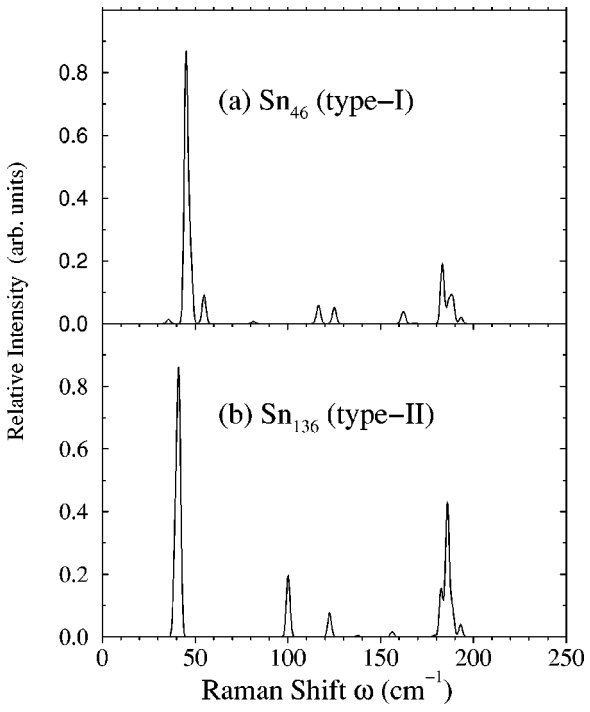

FIG. 2. Raman spectra for (a) Sn_{46} and (b) Sn_{136} calculated using a bond-polarizability model. Parallel polarization, I_{xx}(VV), has been assumed and the intensity has been averaged over a 4π solid angle.

V. TERNARY COMPOUND

A. Lattice vibrational Dispersion relations

As was discussed in Ref. 1, our symmetric, ordered model for $Cs_8Ga_8Sn_{38}$ assumes that there are no Ga-Ga bonds and that the eight Ga atoms occupy half of the 16*i* symmetry sites. The lattice point group symmetry is T_d. Use of this symmetry in the calculation of $\phi(\vec{q}=\vec{0})$ still requires that 18 independent displacements U_0 be made (36 with positive and negative U_0). These consist of three orthogonal displacements for each of the following atoms and symmetry sites: Ga on a 16*i* site, Sn on a 16*i* site, Sn on a 6*c* site, Sn on a 24*k* site, Cs on a 2*a* site, and Cs on a 6*d* site. Group theory generates the remaining $(3\times 54)-18=144$ columns of $\phi(\vec{q}=\vec{0})$.

For $Cs_8Ga_8Sn_{38}$, we have found that the low-lying (''rattling'') vibrational modes of the Cs guests in the large cages are sensitive to the choice of the displacement U_0 used in the calculation of $\phi(\vec{q})$. *For these modes only*, it was necessary to use $U_0=0.03$ Å, in order to obtain a physically realistic phonon spectrum. (For all other modes we used $U_0=0.02$ Å.) For these rattling modes, using $U_0=0.02$ Å resulted in some imaginary frequencies. This artifact is due to the weak bonding of the Cs, which causes the modes associated with it to be extremely anharmonic. To test the sensitivity of these rattling modes to the choice of U_0, we have also computed them using $U_0=0.04$, 0.05, and 0.06 Å. We find that the frequencies change by less than 1% for each 0.01 Å change in U_0. This sensitivity of rattling modes to the choice of U_0 is likely an intrinsic limitation of the harmonic approximation.

In order to better understand the Cs rattling motion, we have also investigated the effective potential energy when a Cs is displaced in a large cage while the framework is kept fixed. The large cage contains 12 pentagons and 2 hexagons of the framework. Visually, it appears ''squashed'' along the *z* axis (the axis through both directly opposite hexagons). An LDA calculation of the effective potential energy for displacements parallel to the *z* axis gives a function that can be fitted to the form $V_\parallel=\frac{1}{2}K_\parallel z^2+\frac{1}{4}\epsilon_\parallel z^4$, where $K_\parallel=1.415$ eV Å^{-2} and $\epsilon_\parallel=1.268$ eV Å^{-4}. A similar calcula-

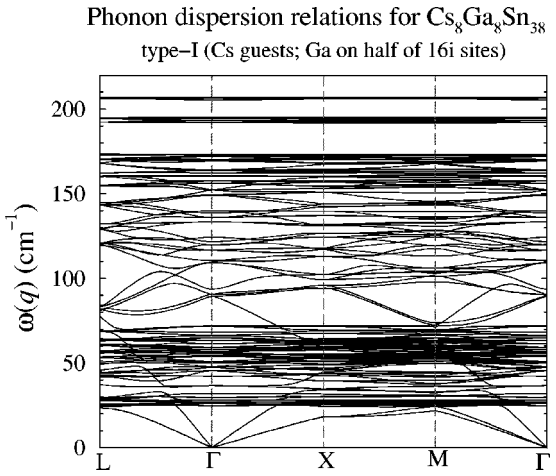

FIG. 3. Phonon dispersion relations for the ternary clathrate compound $Cs_8Ga_8Sn_{38}$.

tion for displacements perpendicular to the z axis (the x direction) results in an effective potential energy $V_\perp = \frac{1}{2}K_\perp x^2 + \frac{1}{4}\epsilon_\perp x^4$, where $K_\perp = 0.226$ eV Å^{-2} and $\epsilon_\perp = 0.534$ eV Å^{-4}. For comparison, a similar calculation for a framework atom yields an almost perfect harmonic effective potential with a ''spring constant'' of $K_{\rm host} \sim 8.0$ eV Å^{-2}. It is thus clear that, in both directions, the Cs potential is very anharmonic and that the effective harmonic ''spring constants'' are very weak in comparison to those for framework atoms. Further, $V_\perp$ is clearly ''softer'' than $V_\parallel$. These results are consistent with the picture of Cs being loose-fitting in an oversized cage. This is an ideal situation for ''rattling'' to occur and for the Cs guests to act as scatterers for low-lying framework acoustic phonons, thus reducing the thermal conductivity.

The vibrational spectrum for our model of $Cs_8Ga_8Sn_{38}$ is shown in Fig. 3. Many features of this are similar to those of Sn_{46}, and the ''parent'' material's modes can be identified by comparing Fig. 3 and Fig. 1(a). For example, the acoustic and optic modes occur in the same regions in the two materials: ~ 0–40 cm^{-1} and ~ 40–190 cm^{-1}. However, there are two interesting regions of the $Cs_8Ga_8Sn_{38}$ spectrum that are not present in that for Sn_{46}.

First, above the optic mode region of Sn_{46}, between ~ 190 cm^{-1} and 210 cm^{-1}, there are two narrow bands of flat, opticlike modes. Because Ga has a smaller atomic mass than Sn ($M_{\rm Sn}/M_{\rm Ga} = 118.69/69.72 \sim 1.7$), we expect that these modes are due to the motions of relatively light Ga atoms in the framework. An analysis of their eigenvectors shows that this expectation is correct.

Second, from ~ 25 to 40 cm^{-1}, a number of flat bands are seen in Fig. 3. This is in the region of the acoustic bands in Sn_{46}. An eigenvector analysis shows that these modes are due to the Cs guest motion in the large and small cages. We thus identify them with the expected low-frequency ''rattling'' modes of the Cs guests. The presence of these modes has also considerably suppressed the width of the acoustic bands in the compound, in comparison with that of Sn_{46}. Because only the lowest-lying acoustic modes have sufficient group velocities to efficiently transfer heat,[39] the presence of these ''rattling'' modes has the potential to suppress the thermal conductivity.

B. $\vec{q}=\vec{0}$ modes; ir and Raman-active modes; theoretical and experimental Raman spectra

The calculated frequencies of the $\vec{q}=\vec{0}$ modes for $Cs_8Ga_8Sn_{38}$ are listed in the first column of Table II. There are 66 distinct theoretical frequencies in Table II that come from $162 = (3 \times 54)$ Γ-point modes. These have the symmetries $5A_1 + 7A_2 + 12E + 20T_1 + 22T_2$. We have used symmetry[43] to determine the ir- and Raman-active modes. These are indicated by a $\surd$ in the appropriate column in Table II.

The calculated Raman spectrum of our model of $Cs_8Ga_8Sn_{38}$ is shown in Fig. 4(a). Results for both parallel polarization I_{xx}(VV) and perpendicular polarization I_{xy}(HV) are shown. In using the BPM discussed Sec. II and Refs. 16 and 18 to compute the spectra for $Cs_8Ga_8Sn_{38}$, we have used the same empirical parameters[37] as those for Sn_{46} and Sn_{136}. That is, the same bond polarization parameter has been assumed for the Ga-Sn bond as for the Sn-Sn bond, ignoring the difference between a Sn-Sn bond and a Ga-Sn bond in this Raman intensity calculation. This reduces the number of parameters in the model, but is not rigorously correct and it may cause underestimates of the intensities of some Raman-active modes.

The theoretical VV and HV spectra are virtually indistinguishable except for the intensity due to the A_1 mode appearing in the VV spectrum at 120.3 cm^{-1}. The peaks at 149.0 cm^{-1} and 206.3 cm^{-1} contain very small intensity A_1 mode contributions that are not resolved from the modes of E and T_2 symmetry at nearly identical shifts. The A_1 mode at 152.5 cm^{-1} is not predicted to exhibit significant Raman intensity. [Compare Fig. 4(a) with Table II.] The VV and the HV spectra are very rich and contain many of the features of the Sn_{46} ''parent'' spectrum [Fig. 2(a)]. Owing to symmetry reduction, some of the degeneracies of the Sn_{46} (O_h symmetry) modes are lifted in the spectrum of $Cs_8Ga_8Sn_{38}$ (T_d symmetry). This makes it difficult to obtain a clear one-to-one mapping of the ''parent'' Sn_{46} peaks to the $Cs_8Ga_8Sn_{38}$ peaks.

In Fig. 4(a), the peaks due to the three low-frequency modes, which our calculations show are clearly rattling modes, are labeled by asterisks. The centers of these peaks have frequencies at 26.0, 31.3, and 35.2 cm^{-1}. An eigenvector analysis of these modes shows that they are due to Cs rattling motion in the large 24-atom cages. The peak at 26.0 cm^{-1} is actually two nearly degenerate peaks (Table II) that are unresolvable. There is a fourth low-frequency peak near 42.4 cm^{-1}. An eigenvector analysis shows that this peak is associated with the framework. There are no low-frequency peaks in the theoretical Raman spectrum that can clearly be associated with Cs motion in the small cages. There is a peak at 54.2 cm^{-1} associated with this motion, but it is hidden under the framework peak at 55.5 cm^{-1}.

For comparison with the theoretical spectra of Fig. 4(a), the low-energy experimental Raman spectrum of

TABLE II. Γ-point ($\vec{q}=\vec{0}$) phonon modes for $Cs_8Ga_8Sn_{38}$. The unique frequencies are listed, along with their symmetries. Also listed are their predicted VV polarization Raman intensities on a scale normalized so that the maximum is 1.0. The symmetry-defined Raman or ir activity of each mode is denoted by a check mark ($\surd$) in the appropriate column. Modes that are primarily due to Cs guest (rattler) motion in the large and small cages are labeled (L) and (S). The observed experimental frequencies are associated with modes as listed. The experimental peak at 19 cm^{-1}, which is assigned to the theory modes at 26.0 and 26.9 cm^{-1}, is observable in the HV spectrum. The remainder of the experimental peaks were taken from the VV spectrum. Several theoretical peaks may not be experimentally resolved and therefore are listed with a common fit frequency.

Predicted frequency (cm^{-1})	Predicted VV intensity	Experimental frequency (cm^{-1})	Symmetry	Raman active	ir active
25.0	0		T_1 (L)		
26.0	0.53	19	T_2 (L)	$\surd$	$\surd$
26.9	0.05	19	T_2 (L)	$\surd$	$\surd$
28.0	0		T_1 (L)		
31.3	0.19	26	E (L)	$\surd$	
32.1	0		A_2 (L)		
35.2	0.07	37	T_2 (L)	$\surd$	$\surd$
42.4	0.06	47	T_2	$\surd$	$\surd$
47.7	0		T_1 (S)		
49.4	0		T_1		
50.3	0		T_1		
51.7	0		E	$\surd$	
54.2	0.06	60	T_2 (S)	$\surd$	$\surd$
55.5	1.00	60	T_2	$\surd$	$\surd$
56.7	0		A_1	$\surd$	
56.8	0		T_1		
56.9	0		T_1		
57.3	0.16	60	E	$\surd$	
59.2	0.56	60	T_2	$\surd$	$\surd$
60.4	0.42	60	E	$\surd$	
63.2	0.02		T_2	$\surd$	$\surd$
64.1	0.03		T_2	$\surd$	$\surd$
64.2	0		T_1		
65.2	0		T_1		
65.8	0		A_2		
69.9	0.38	60	T_2	$\surd$	$\surd$
87.7	0		E	$\surd$	
89.0	0		T_1		
90.6	0		A_2		
109.7	0.09	122	T_2	$\surd$	$\surd$
110.4	0.09	122	E	$\surd$	
117.4	0.06	122	T_2	$\surd$	$\surd$
120.3	0.12	115	A_1	$\surd$	
120.9	0		T_1		
124.1	0		A_2		
134.1	0		T_1		
136.2	0		T_1		
139.1	0		A_2		
140.3	0.03	141	T_2	$\surd$	$\surd$
148.4	0.26	131	E	$\surd$	
149.0	0.05	131	A_1	$\surd$	
151.9	0		T_2	$\surd$	$\surd$
152.5	0		A_1	$\surd$	

TABLE II. *(Continued)*

Predicted frequency (cm^{-1})	Predicted VV intensity	Experimental frequency (cm^{-1})	Symmetry	Raman active	ir active
155.2	0.06	161	T_2	√	√
156.7	0		T_1		
160.8	0		T_1		
162.4	0.52	161	E	√	
163.6	0		T_2	√	√
165.0	0.01		E	√	
169.0	0		T_1		
170.1	0.07	175	T_2	√	√
171.8	0.20	181	E	√	
172.6	0		A_2		
173.2	0.04	181	T_2	√	√
173.6	0		T_1		
192.1	0		T_1		
192.2	0.05	196	T_2	√	√
193.0	0.13	196	E	√	
194.7	0.16	196	T_2	√	√
195.3	0		T_1		
196.2	0.14	196	E	√	
206.3	0.24	203	T_2	√	√
206.3	0.01		A_1	√	
206.7	0		A_2		
207.4	0		T_1		

$Cs_8Ga_8Sn_{38}$, taken at 10 K, is shown in Fig. 4(b) for HV polarization and in Fig. 4(c) for VV polarization. The experimental spectra were measured under nonresonant conditions using green ($\lambda = 514.5$ nm) light. The open squares depict the data, the bold curve shows the complete fit function, and the thin curves indicate individual Lorentzian peak functions. The overall background was removed by subtracting a smooth function. The fitting routine requires that starting peak values be input manually, but all parameters are allowed to vary during the iterative convergence process. While the agreement between the theoretical and experimental spectra is not perfect, especially for the relative intensities of some peaks, it is clear upon comparison of Figs. 4(a), 4(b), and 4(c) that the calculated spectra contain most of the main qualitative features of the experimental spectra. The positions of most of the peaks are very well predicted by the theory. The peaks in the experimental VV spectrum of Fig. 4(c), which are identified as A_1 and occur at 115 cm^{-1} and 131 cm^{-1}, display significantly larger intensity in the VV spectrum than in the HV spectrum.

The most significant quantitative comparison between the theoretical and experimental Raman spectra can be made for the low-frequency, rattler-derived vibrational modes. The experimental spectrum has *four* low-frequency peaks at 19, 26, 37, and 47 cm^{-1}, which can be directly compared with the *four* theoretical low-frequency Raman modes at 26.0, 31.3, 35.2, and 42.4 cm^{-1}. Theoretically, only the three lowest modes have eigenvectors that show they are produced by Cs motion within the large (24-atom) cage; the highest frequency mode at 42.4 cm^{-1} is framework-derived. The three lowest-frequency experimental peaks at 19, 26, and 37 cm^{-1} compare well with the frequency range of these theoretical rattler modes. There is uncertainty as to whether the experimental peak at 47 cm^{-1} is a rattler or a framework mode. Either can be accounted for within the current theory. Overall, this combination of theoretical and experimental analyses produces a convincing picture that the lowest three observed peaks in the experimental spectrum are rattling modes due to Cs motion in the large cages. Also, based on the above analysis, the high-frequency peaks in the range 192 cm^{-1} to 206 cm^{-1} are due to the motion of the lighter Ga atoms in the framework.

In Table II, we qualitatively (semiquantitatively) compare the predicted and measured Raman spectra. In the second column of that table, we list the predicted VV polarization intensities, I_{xx}, for the Raman-active modes on a relative scale with the maximum peak normalized to an intensity of 1.0. In the third column, we associate the experimentally observed Raman modes with the predicted ones. We list the frequency of each observed phonon beside a predicted mode based on the best theoretical-experimental match of frequency, intensity, and symmetry. By this means, we are able to associate observed peaks with specific, predicted Raman-active modes. We note that, due to the broadness of some experimental peaks, several theoretical peaks may not be experimentally resolved. These are therefore listed with a common experimental frequency. In addition, some theoretical Raman-active modes have predicted relative intensities that are too small to be observed experimentally. These are therefore not associated with experimental frequencies in Table II.

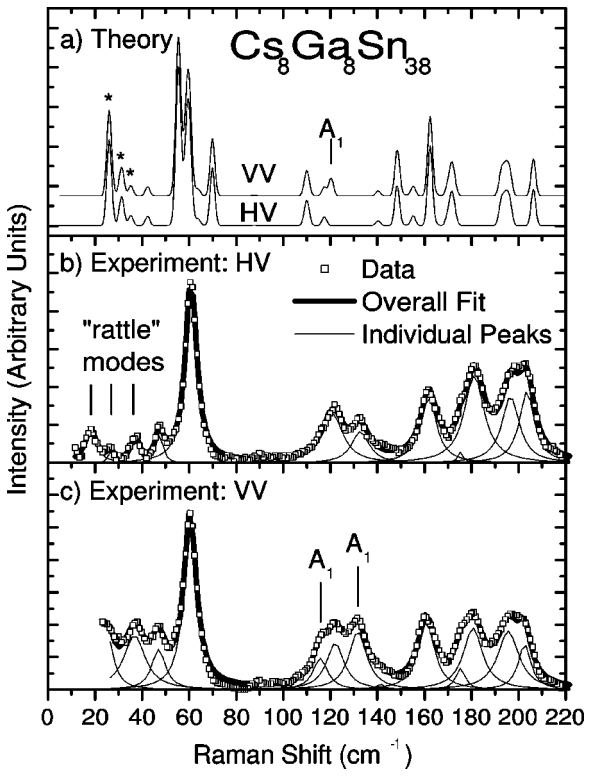

FIG. 4. The Raman spectrum of $Cs_8Ga_8Sn_{38}$. (a) Theoretical calculations for the Raman intensity in VV and HV polarizations. An asterisk indicates Cs-rattling modes. (b) Measured low-energy Raman spectrum taken at 10 K using $\lambda = 514$ nm in HV polarization. (c) Measured spectrum taken in VV polarization. In (b) and (c) the open squares represent data points, the thick curve is the overall fit, and the thin curves show individual peaks from the fit. The short vertical lines indicate the low-frequency ''rattle'' modes.

The criteria used to make the assignments of the experimental peaks to the theory modes were the following. Starting at the lowest frequencies, the experimental peak at 19 cm^{-1}, which is assigned to the theory modes at 26.0 and 26.9 cm^{-1}, is observable in the HV spectrum. The remainder of the experimental peaks in the table were taken from the VV spectrum. Moving up in frequency, we have made assignments using the predicted intensity as a guide and have attempted to match experimental peaks with theoretical modes as near to them in frequency as possible. In order to match the experimental peak at 115 cm^{-1}, which is identified as A_1-symmetric in Fig. 4(c), with the theoretical A_1-symmetric mode at 120.3 cm^{-1}, we have had to slightly deviate from this procedure and to ''invert'' the order of the assignments by identifying the experimental peak at 122 cm^{-1} with the three theoretical peaks (T_2-, E-, and T_2-symmetric) at 109.7, 110.4, and 117.4 cm^{-1}. Similarly, we have identified the experimental A_1-symmetric peak at 131 cm^{-1} with the theoretical A_1 peak at 149.0 cm^{-1}, while identifying the experimental peak at 141 cm^{-1} with the two theoretical (T_2 and E) peaks at 140.3 and 148.4 cm^{-1}.

With the exception of the low-frequency Cs, ''rattler'' modes and the high-frequency Ga modes, the majority of the theoretical-experimental comparisons in Table II should be viewed as qualitative. This is particularly true since the calculations have assumed an ordered, high-symmetry model of $Cs_8Ga_8Sn_{38}$, while the experimental sample was a polycrystalline material with the Ga ''alloyed'' into the Sn framework. Given this fact, the good agreement between theory and experiment seen in Table II and, especially, in Fig. 4 is somewhat remarkable. We speculate that this agreement may be an indication that there might have been some ordering in the experimental sample.

VI. CONCLUSIONS

Starting with previously obtained[1] LDA-optimized structures for Sn-based clathrates, we have performed an LDA-based study of the vibrational properties of the pure framework clathrate materials Sn_{46} and Sn_{136} and in the ternary compound $Cs_8Ga_8Sn_{38}$. For Sn_{46} and Sn_{136}, the acoustic modes are in the range 0–40 cm^{-1} and most optical modes have small group velocities. In $Cs_8Ga_8Sn_{38}$ we find ''rattling'' phonon modes, due to the Cs motion, in the range 18–37 cm^{-1}, in good agreement with Raman data. These modes reduce the acoustic phonon band width of $Cs_8Ga_8Sn_{38}$ in comparison with that of Sn_{46}. They thus have the potential to scatter the low-lying, heat-carrying acoustic modes of the framework, and thus to lower the thermal conductivity.

We have also predicted the ir- and Raman-active phonon modes in these materials, and have predicted the Raman spectra using a bond-polarizability model. In addition, we have performed Raman scattering experiments on $Cs_8Ga_8Sn_{38}$ and have found that the calculated spectra are in reasonable agreement with experiment. Finally, we have identified three low-frequency Raman peaks as coming from the rattling of Cs in the 24-atom cages. We hope that our predictions will prove useful in interpreting future experiments.

ACKNOWLEDGMENTS

We thank the NSF for support (Grant Nos. DMR-99-86706 and DMR-96-32635) which supported this work. We thank Dr. G. Ramachandran and Professor P. McMillan, Professor R. Marzke, and Professor J. Gryko for helpful discussions. C.W.M. thanks Texas Tech for a Development Leave which enabled him to carry out a portion of this work and Arizona State for their hospitality while a portion of the work was done. J.D. acknowledges support from his Auburn start-up fund and thanks Professor A.-B. Chen for insightful discussions. Work by C.K. at NRL is supported by the ONR. Sample preparation was conducted at Marlow Industries under the ARL SBIR Phase II Grant No. DAAD17-99-C-006. G.S.N. thanks the University of South Florida for support.

[1] C.W. Myles, J.J. Dong, and O.F. Sankey, Phys. Rev. B **64**, 165202 (2001).
[2] J.S. Kasper, P. Hagenmuller, M. Pouchard, and C. Cros, Science **150**, 1713 (1965).
[3] C. Cros, M. Pouchard, and P. Hagenmuller, C.R. Hebd. Sci. Seances Acad. Sci. **260**, 4764 (1965).
[4] C. Cros, M. Pouchard, P. Hagenmuller, and J.S. Kasper, Bull. Soc. Chim. Fr. **7**, 2737 (1968).
[5] C. Cros, M. Pouchard, and P. Hagenmuller, J. Solid State Chem. **2**, 570 (1970); Bull. Soc. Chim. Fr. **2**, 379 (1971).
[6] J. Gryko, P.F. McMillan, R.F. Marzke, A.P. Dodokin, A.A. Demkov, and O.F. Sankey, Phys. Rev. B **57**, 4172 (1998); G.K. Ramachandran, J. Dong, J. Diefenbacher, J. Gryko, O.F. Sankey, R.F. Marzke, M. O'Keeffe, and P.F. McMillan, J. Solid State Chem. **145**, 716 (1999).
[7] S. Bobev and S.C. Sevov, J. Am. Chem. Soc. **121**, 3795 (1999).
[8] J.-T. Zhao and J.D. Corbett, Inorg. Chem. **33**, 5721 (1994).
[9] G.S. Nolas, T.R.J. Weakley, and J.L. Cohn, Chem. Mater. **11**, 2470 (1999); J.L. Cohn, G.S. Nolas, V. Fessatidis, T.H. Metcalf, and G.A. Slack, Phys. Rev. Lett. **82**, 779 (1999).
[10] G.S. Nolas, B.C. Chakoumakos, B. Mahieu, G. Long, and T.R.J. Weakley, Chem. Mater. **12**, 1947 (2000).
[11] G.S. Nolas and C.A. Kendziora, Phys. Rev. B **62**, 7157 (2000).
[12] G.B. Adams, M. O'Keeffe, A.A. Demkov, O.F. Sankey, and Y. Huang, Phys. Rev. B **49**, 8048 (1994).
[13] A.A. Demkov, O.F. Sankey, K.E. Schmidt, G.B. Adams, and M. O'Keeffe, Phys. Rev. B **50**, 17001 (1994).
[14] S. Saito and A. Oshiyama, Phys. Rev. B **51**, R2628 (1995).
[15] V.I. Smelyansky and J.S. Tse, Chem. Phys. Lett. **264**, 459 (1997).
[16] J. Dong, O.F. Sankey, and G. Kern, Phys. Rev. B **60**, 950 (1999).
[17] P. Mélinon, P. Keǵhelian, X. Blase, J. LeBruse, A. Perez, E. Reny, C. Cros, and M. Pouchard, Phys. Rev. B **58**, 12590 (1998).
[18] J. Dong and O.F. Sankey, J. Phys.: Condens. Matter **11**, 6129 (1999).
[19] N.P. Blake, L. Mollnitz, G. Kresse, and H. Metiu, J. Chem. Phys. **111**, 3133 (1999).
[20] G.A. Slack, in *Thermoelectric Materials—New Directions and Approaches*, edited by T.M. Tritt, G. Mahan, H.B. Lyon, Jr., and M.G. Kanatzidis, Mater. Res. Soc. Symp. Proc. No. 478 (Materials Research Society, Pittsburg, PA, 1997), p. 47.
[21] G.A. Slack, in *CRC Handbook of Thermoelectrics*, edited by D.M. Rowe (CRC, Boca Raton, FL, 1995), p. 407.
[22] T.M. Tritt, Science **283**, 804 (1999).
[23] L. Mihaly, Nature (London) **395**, 839 (1998); V. Keppens, D. Mandrus, B. Sales, B. Chakoumakos, P. Dai, R. Coldea, M. Maple, D. Gajewski, E. Freeman, and S. Bennington, *ibid.* **395**, 876 (1998).
[24] G.S. Nolas, D.T. Morelli, and T.M. Tritt, Annu. Rev. Mater. Sci. **29**, 89 (1999).
[25] G.S. Nolas, J.L. Cohen, G.A. Slack, and S.B. Schujman, Appl. Phys. Lett. **73**, 178 (1998).
[26] J. Dong, O.F. Sankey, C.W. Myles, G.K. Ramachandran, P.F. McMillan, and J. Gryko, in *Thermoelectric Materials 2000*, edited by T.M. Tritt, G.S. Nolas, G. Mahan, M.G. Kanatzidis, and M. Mandrus, Mater. Res. Soc. Symp. Proc. Proceedings No. 626 (Materials Research Society, San Franciso, 2000), p. Z6.1.1.
[27] J. Dong, O.F. Sankey, and C.W. Myles, Phys. Rev. Lett. **86**, 2361 (2001).
[28] G.S. Nolas, T.J.R. Weakley, J.L. Cohn, and R. Sharma, Phys. Rev. B **61**, 3845 (2000).
[29] D. Vanderbilt, Phys. Rev. B **41**, 7892 (1990); K. Laasonen, R. Car, C. Lee, and D. Vanderbilt, *ibid.* **43**, 6796 (1991).
[30] G. Kresse and J. Hafner, J. Phys.: Condens. Matter **6**, 8245 (1994); G. Kresse and J. Hafner, Phys. Rev. B **48**, 13 115 (1993).
[31] This program was developed at the Institut für Theoretiche Physik of the Technische Universität Wien. G. Kresse and J. Furthmüller, Comput. Mater. Sci. **6**, 15 (1996).
[32] G. Kresse and J. Hafner, Phys. Rev. B **47**, 558 (1993); G. Kresse and J. J. Furthmüller, *ibid.* **54**, 11169 (1996).
[33] D.M. Ceperley and B.J. Alder, Phys. Rev. Lett. **45**, 566 (1980).
[34] In reporting the Raman and ir modes in this work, we use the results computed exactly for the $\vec{q}=\vec{0}$ force constant matrix, and not the approximate values obtained by determining the short-ranged real-space force constant matrix and transforming back to reciprocal space. If we use the approximate matrix at $\vec{q}=\vec{0}$, a maximum error of 5 cm^{-1} is found.
[35] S. Go, H. Blitz, and M. Cardona, Phys. Rev. Lett. **34**, 121 (1975).
[36] D.W. Snoke and M. Cardona, Solid State Commun. **87**, 121 (1993).
[37] In this study, we use $\alpha_1/\alpha_q=-1.0$ and $\alpha_{25}/\alpha_q=-0.35$.
[38] J.J. Dong, O.F. Sankey, G.K. Ramachandran, and P.F. McMillan, J. Appl. Phys. **87**, 7726 (2000).
[39] N.W. Ashcroft and N.D. Mermin, *Solid State Physics* (Holt, Reinhart, and Winston, New York, 1976), p. 500.
[40] Y. Guyot, B. Champagnon, E. Reny, C. Cros, M. Pouchard, P. Melinon, A. Perez, and I. Gregora, Phys. Rev. B **57**, R9475 (1997).
[41] A.A. Demkov, O.F. Sankey, S. Daftuar, and J. Gryko, in *Proceedings of the International Conference on the Physics of Semiconductors*, edited by P.J. Lockwood (World Scientific, New Jersey, 1994), p. 2205.
[42] W. Weber, Phys. Rev. B **15**, 4789 (1977).
[43] W.G. Fateley, F.R. Dollish, N.T. McDevitt, and F.F. Bently, *Infrared and Raman Selection Rules for Molecular and Lattice Vibrations: The Correlation Method* (Wiley-Interscience, New York, 1972).